Methods documentation for "Three subject-specific human tibiofemoral joint finite element models: complete three-dimensional imaging (CT & MR), experimental validation and modelling dataset." Cooper et al, 2023, https://doi.org/10.5518/981

Research Project: *Optimising knee therapies through improved population stratification and precision of the intervention*

Summary of tissue dissection cases and overview of process

- Computational model predictions were compared with experimental measurements of the tibiofemoral joint with the menisci in place and with them both removed (**Figure 1**).
- Cadaveric knee specimens were imaged using MR in their fully intact state, before being dissected down to the tibiofemoral joint and cemented into pots for static loading and contact mechanics measurements.
- The first set of measurements were taken with both menisci in place and a second set of measurements were taken after a double meniscectomy.
- After all testing, the tibia and femoral bones were imaged separately in a micro-CT scanner.
- Computational model bone and cartilage shape was derived from the micro-CT images.
- For the cases where the menisci were included, the MR images were used to define the meniscus shape.
- A set of computational cases where the cartilage thickness was location specific were generated by segmenting the cartilage layers from the micro-CT image.
- A second set of cases were created, where the cartilage layer had a uniform thickness.
- Both the "location specific" and the "uniform thickness" cartilage cases were generated for the "double meniscectomy" scenario.
- Only the "location specific" cases where generated for the "intact menisci" case.

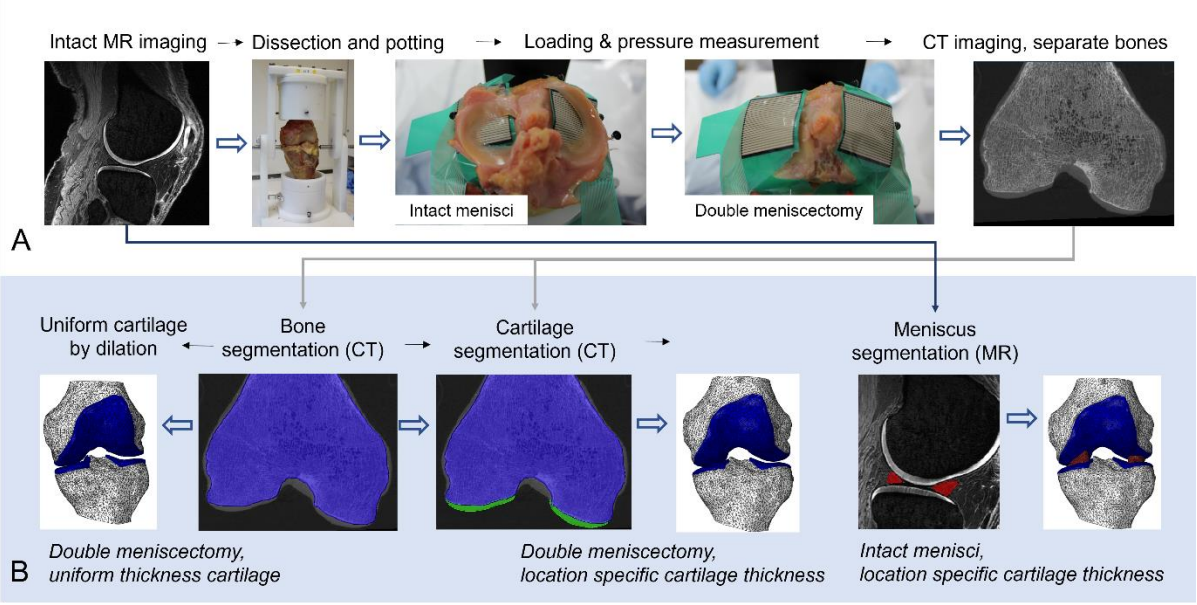

Figure 1. An overview of **A)** the experimental protocol and **B)** the development steps for the three geometric states of the computational models.

Imaging and experimental methods

Specimen details, pre-test imaging & freeze thaw cycles

- Following ethical approval (East Midlands - Leicester South Research Ethics Committee (18/EM/0224)), three fresh-frozen human cadaveric knees (**Table 1**) were obtained and stored at – 40 °C.
- Each whole knee was defrosted in the fridge for at least 48 hours before magnetic resonance (MR) imaging on a 3 Tesla MR scanner (Siemens Magnetom Prisma, Erlangen, Germany) using a 15 channel transmit/receive knee coil (Siemens, Erlangen, Germany), and employing a 3D Double Echo Steady State sequence, at a resolution of 0.36 x 0.36 x 0.7 mm^3.
- All knees were MR imaged in their intact state and without any tissue manipulation, after which they were returned to - 40 °C storage.
- The defrosting regime was performed again before each knee was dissected.

Table 1. Details of the three human donor knees.

Donor	Knee	Sex	Age	BMI (kg/m^2)	Soft tissue condition
1	Right	Male	57	38.1	Signs of cartilage and lateral meniscus degeneration
2	Left	Male	61	18.0	No meniscal extrusion.
3	Left	Male	81	23.7	Meniscus calcification.

Specimen dissection & alignment for testing

- The patella was removed, along with the majority of soft tissues, retaining the articular cartilage, the menisci and the posterior capsular tissues. The latter was retained as they prevented over extension of the tibiofemoral joint during manipulations and potting.
- Established methods were used to locate an axis of femoral flexion and drill small holes on either side of the femoral condyles (Liu et al., 2019).
- The femur and tibia were then cemented in custom-built pots using polymethylmethacrylate (PMMA; WHW Plastics, UK), using a rig the same size of the testing set up.
- As much as possible of the tibial and femoral shafts were retained above and below the axis of rotation.
- The posterior capsular soft tissue was resected following potting.

Experimental constraints & loading

- Each potted knee was placed in a custom rig (Cooper et al., 2020), where the femur was constrained in all degrees of freedom except for superior-inferior translation.
- Two cases of tibial constraint were tested: one “fully constrained” and one “partially freed”, where the tibia was allowed to move in three degrees of freedom, namely anterior-posterior translation, internal-external rotation and abduction-adduction (**Figure 2**).
- Each knee was axially loaded in a material testing machine (Instron 3365 with a 5 kN load cell, Instron, UK).
- An axial compression was slowly increased (1 mm / minute) up to 500 N and then held for 60 seconds.
- Contact pressures were recorded at this time point, allowing the tissue to settle.
- For the case with three degrees of tibial freedom on Knee 2, the full 500 N load could not be achieved since a large amount of anterior displacement meant that the experiments had to be terminated to avoid dislocation.
- Results at the maximum possible loads were therefore recorded for Knee 2; 200 N for the intact menisci case and 80 N for the double meniscectomy case.

Experimental pressure measurements

- Experimental contact pressure measurements were obtained using thin film pressure sensors (Tekscan Pressure Mapping Sensor Model 4000, Tekscan Inc., Boston, MA, USA), inserted from the posterior and underneath the menisci, and fixed using pins anteriorly and posteriorly.
- Prior to testing, the pressure sensors were conditioned and calibrated using the Tekscan software I-Scan against a pre-calibrated load cell (Instron, UK) rated to 5 kN.
- A new pressure sensor was used for each knee specimen to minimise error resulting from deformation of the sensors when positioned on the uneven knee joint surfaces.
- Additionally, the tissue and sensors were allowed to relax between each loading test, for a time equivalent to five times the load duration.

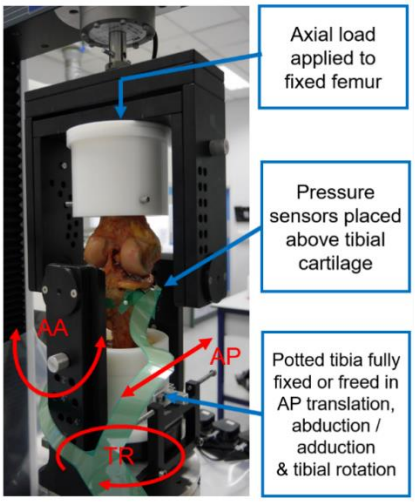

Figure 2: Example of the set up for the experimental tests showing a human tibiofemoral joint specimen in the custom designed rig and placed in a material testing machine, with pressure sensors used to measure contact pressures. The three degrees of freedom which can be released on the tibial side are adduction-abduction rotation (AA), tibial rotation (TR) and anterior-posterior translation (AP).

Post-test imaging

- Each bone was imaged again after testing using high-resolution peripheral quantitative computed tomography (XtremeCT, Scanco Medical AG, Switzerland) at an isotropic voxel size of 82 µm.
- At this stage the menisci had been removed and the femur and tibia were separated in the scanner to aid cartilage segmentation from these images.
- The drill holes indicating the femoral flexion axis and cement layers aligned with the experimental pots could be seen in the images, facilitating computational joint alignment.

Modelling methods

Model geometry definition from images

- Femoral and tibial bones and cartilage layers for each knee were segmented from post-meniscectomy CT images using Simpleware ScanIP 2019.09 (Synopsys, Mountain View, CA, USA).
- This segmentation used thresholding followed by morphological operations and Gaussian smoothing for noise removal.
- The relative alignment of the tibia and femur bones was established from features visible on the CT images, including the experimental femoral flexion axis (drill holes) and the axial plane for each bone (cement layer).
- MR images were registered to the CT images within the ScanIP software.
- The MR images were used to approximate the remaining bone alignment and to segment the meniscus geometries for the “intact menisci” cases.
- The manual meniscus segmentation was adjusted to ensure conformity of contact surfaces using dilation, binary operations and curvature adjustments where necessary. This adjustment was required to ensure the model solutions would converge.
- The geometry of the cartilage layers in the “intact menisci” cases matched those in the “double meniscectomy” cases with “location specific” cartilage thickness.
- In the “uniform thickness” cases, the cartilage was generated by dilating out the bone masks in the regions where cartilage was visible.
- The uniform thickness value was found separately for the femur and tibia of each knee, based on the observed averages on CT images.

Finite element model settings – analysis type

- Finite element models of each case were developed in Abaqus 2017 (Dassault Systèmes, Vélizy-Villacoublay, France) by importing meshed geometries from ScanIP.
- All the FE models developed for this study were static analyses, with geometric non-linearity and unsymmetric matrix storage.

Finite element model settings – mesh selection & computational cost

- All tissue masks were meshed with quadratic tetrahedral elements.
- Mesh sensitivity testing conducted in a previous porcine study showed low sensitivity of peak pressure to element size.
- Doubling the number of elements, equivalent to a 20% reduction in element edge length, resulted in a 1% change in peak contact pressure, a 3% change in mean pressure, and 2% change in contact area.
- In this human tissue work, the average element edge lengths in the collagenous tissues were consistently smaller than in the porcine work (1.1 - 1.2 mm, compared to 1.3 mm for porcine) (Cooper et al., 2020).

- The cartilage thickness was similar to the porcine models when a uniform thickness was used and thicker in the load bearing areas of the cases with location-specific thickness.
- Overall, the models contained approximately 180,000 elements, of which 110,000 elements were for the cartilaginous soft tissues.
- The mesh density was considered a good compromised between precision and computational cost.
- The mean runtimes for cases with a fully constrained tibia and partially freed tibia were 3 hours and 9 hours respectively.

Finite element model settings – material and contact properties

- Bones were modelled as homogeneous, linearly elastic representing much stiffer behaviour than the soft tissues.
- The femoral and tibial cartilage layers were modelled as Neo-Hookean hyperelastic materials.
- The menisci were modelled as transversely isotropic linearly elastic materials, with a higher modulus in the circumferential direction in which the fibrous tissue is aligned.
- All material constants are given in **Table 2**.
- To restrict meniscal movement and represent the meniscus roots, the menisci were attached to the tibial plateau using 15 linear spring elements attached to nodes at each of the four meniscal horn attachment sites.
- The equivalent modulus of the springs over their attached area was of the same order as the meniscus fibre modulus.
- Frictional hard contact enforced using the penalty method was defined between femoral and tibial cartilages ($\mu = 0.1$), and between the meniscus and both cartilage layers, with a higher coefficient of friction ($\mu = 0.15$).

Table 2: Material property parameters and values for the bone, cartilage and menisci.

Bone property values	**Menisci property values**
Young's modulus E = 15 GPa Poisson's ratio ν = 0.3	Elastic moduli $E_{radial} = E_{axial} = 6$ MPa, $E_{circ} = 21$ MPa Poisson's ratios $\nu_{radial\text{-}circ} = \nu_{axial\text{-}circ} = 0.3$, $\nu_{radial\text{-}axial} = 0.2$ Shear moduli $G_{radial\text{-}circ} = G_{axial\text{-}circ} = 2.5$ MPa, $G_{radial\text{-}axial} = 8.08$ MPa
Cartilage property values	
$C_{10} = 1.0274$ MPa $D_1 = 0.08$	

Finite element model settings – constraint and load cases

- The experimental constraint cases and loads were replicated in each knee model.
- Two reference points were placed at the same point on the femoral axis of rotation.
- One reference point was linked through kinematic coupling to the nodes on top surface of the femur and used to apply the femoral constraints and for the application of a concentrated compressive force in the superior-inferior direction.
- The other reference point was coupled to the nodes on the inferior surface of the tibia and used to apply the tibial constraints.
- In the "partially freed" case, the solution would not converge consistently if all three tibial degrees of freedom were unconstrained in the same analysis step. Therefore, each tibial degree of freedom was applied in a separate step, while all other degrees of freedom were constrained, and the resulting displacements and rotations where inherited and modified from step to step.
- Four loading steps were used in the order: adduction-abduction; anterior-posterior displacement; internal-external rotation; and adduction-abduction once again.
- Metrics were taken from the final step.

Measurements and analysis

The analyses in this study are detailed below and summarised in **Table 3**.

The experimental-computational comparisons for "double meniscectomy" cases with "fully constrained" tibial bone

- The pressure distribution on the tibial cartilage (qualitative)
- The balance of force between the two condyles (%)
- The contact area on the tibial cartilage (mm^2)

Where all measures are dependent on the alignment of the two bones, as well as the geometry and material properties input.

- The size of the Tekscan sensels (1.27 mm) limit the precision of the contact area measurements.
- The experimental contact area data is presented as the total area of all sensels with non-zero pressure and an error bar indicating the area of the sensels on the edge of the contact region, providing a band within which the true area falls.

The experimental-computational comparisons for "double meniscectomy" cases with "partially freed" tibial bone

- The pressure distribution on the tibial cartilage (qualitative)
- The balance of force between the two condyles (%)
- The contact area on the tibial cartilage (mm^2)

Where all measures are dependent the geometry and material property settings, but relatively independent of initial bone alignment.

To provide context for the results above **the movement of the tibia is then analysed in the "double meniscectomy", "partially freed" computational case**

- Anterior-posterior translation
- Adduction-abduction angle change
- Internal-external angle change

The experimental-computational comparisons for "intact menisci" cases with both tibial constraints

- Use of the pressure data to assess the contact area and balance of loading between the tibial condyles was dependent on how much of the contact area could be captured on the sensors.
- The presence of the meniscus caused substantial contact outside the sensor area.
- Therefore, a more restricted comparison is made between the computational and experimental pressure distribution (qualitative only) for the intact menisci cases.

Computational only analysis of the meniscus role in the "intact menisci" cases

- The role of the menisci is investigated computationally by comparing the percentage of tibial contact area and percentage of force transferred to the tibia for which the menisci are responsible.
- For the computational cases including both menisci, the percentage of the tibial cartilage contact area which comes from contact with the meniscus and the proportion of the load in each condyle transferred through the meniscus were calculated.

Table 3: *A list of the analyses conducted, including where comparisons are made between computational and experimental data (exp-comp) and where only computational data is used (comp-only), the tissue inclusion cases and tibial constraint cases used, and the metrics used in each analysis. Abbreviations: 'qual' = qualitative assessment; and 'men. %' = the percentage of the total measure for which the meniscus is responsible.*

Analysis type	**Tissue inclusion**	**Tibial constraint**	**Pressure dist. (qual)**	**Force balance**	**Contact area**	**Tibial movement**	**Contact area (men. %)**	**Force (men. %)**
Exp-comp	double meniscectomy	fully constrained	Y	Y	Y			
Exp-comp	double meniscectomy	partially freed	Y	Y	Y			
Comp-only	double meniscectomy	partially freed				Y		
Exp-comp	intact menisci	both	Y					
Comp-only	intact menisci	both					Y	Y

Thickness analysis of the cartilage in the three knees for context

- In modelling cases where the cartilage thickness was location-specific, the thickness varied by between 0.1 and 1.1 mm, depending on the specimen and the cartilage area.
- Knee 2 had the most consistent cartilage thickness overall, followed by knee 3, and knee 1 had the largest variation in thickness.
- The use of CT images of the separated tibial and femoral bones allowed for a consistent segmentation process, with little user-dependency.
- The majority of the thickness variation could therefore be captured with confidence when segmenting an image with a resolution of 0.164 x 0.164 x 0.164 mm^3, with some finer aspects of thickness variation (e.g. areas of knee 2) likely being lost to image resolution.

Cartilage material properties calibration

To approximate the possible range of material property values for cartilage in theses cadaveric knee joints, the cartilage modulus was calibrated to match the total contact area measured experimentally. This was done in the double meniscectomy cases with the partially freed tibia and using the computational models with non-uniform segmented cartilage. Adjustments were made to the material properties of the cartilage until the difference between the experimental and computational contact areas were less than 8%. The process was performed separately for each of the three models.

The resulting equivalent Young's modulus of the cartilage was different for each model, with a maximum difference of 1 MPa and an average value of 4 MPa **(Table 4**).

Table 4: *Cartilage material properties calibrated separately for each knee, based on match to the contact area observed experimentally in the segmented cartilage meniscectomy cases with a partially freed tibia.*

Cartilage materials properties	**Assumed (above)**	**Knee 1**	**Knee 2**	**Knee 3**
Equivalent linear Young's modulus (MPa, assuming ν=0.46)	6	4.5	3.5	4
C_{10} (MPa)	1.0274	0.7705	0.5993	0.6849
Bulk modulus (K, in MPa)	25	18.75	14.6	16.67

References

Cooper, R.J., Liu, A., Day, G.A., Wijayathunga, V.N., Jennings, L.M., Wilcox, R.K., Jones, A.C., 2020. Development of robust finite element models of porcine tibiofemoral joints loaded under varied flexion angles and tibial freedoms. Journal of the Mechanical Behavior of Biomedical Materials, 109, 103797, https://doi.org/10.1016/j.jmbbm.2020.103797

Liu, A., Ingham, E., Fisher, J., Jennings, L.M., 2019. Development of a pre-clinical experimental simulation model of the natural porcine knee with appropriate ligamentous constraints. PLoS One 14, e0216872. https://doi.org/10.1371/journal.pone.0216872